Optics Letters

Super-resolution stimulated emission depletion microscopy of director structures in liquid crystals

Jung-Shen B. Tai[1] and Ivan I. Smalyukh[1,2,3,*]

[1]Department of Physics, University of Colorado, Boulder, Colorado 80309, USA
[2]Materials Science and Engineering Program, Soft Materials Research Center and Department of Electrical, Computer and Energy Engineering, University of Colorado, Boulder, Colorado 80309, USA
[3]Renewable and Sustainable Energy Institute, National Renewable Energy Laboratory and University of Colorado, Boulder, Colorado 80309, USA
*Corresponding author: ivan.smalyukh@colorado.edu

Received 24 August 2018; revised 19 September 2018; accepted 24 September 2018; posted 24 September 2018 (Doc. ID 343142); published 15 October 2018

Extending the optical imaging of director structures in liquid crystals (LCs) beyond the diffraction limit is poised to provide insights into previously elusive LC physics at the nanoscale. Here, we develop and characterize super-resolution stimulated emission depletion (STED) microscopy with molecular orientation sensitivity and apply it to reveal spatially localized director structures in chiral nematic and smectic LCs. As examples, we demonstrate director imaging and reconstruction of nanoscale LC configurations, including solitonic Bloch walls and two-dimensional skyrmions, both observed in sub-micrometer-thick strongly confined LC films, and focal conic domains in smectic LCs. The $\lesssim$100 nm resolution of our orientation-resolved STED imaging is three times better than that of fluorescence confocal polarizing microscopy and polarized nonlinear imaging techniques, but can be potentially improved even further.

https://doi.org/10.1364/OL.43.005158

Liquid crystals (LCs) with long-range orientational order and partial or no positional order exhibit a rich variety of complex three-dimensional spatial patterns, described by the director $\boldsymbol{n} \equiv -\boldsymbol{n}$, the local average molecular orientation [1]. Noninvasive optical imaging of $\boldsymbol{n}(\boldsymbol{r})$ has been often utilized to unambiguously identify the detailed director structures in LCs, important for both fundamental LC research and technological applications [1]. In fluorescence confocal polarizing microscopy (FCPM), LCs are doped with anisotropic fluorescent dyes whose transition dipoles of absorption and emission follow $\boldsymbol{n}(\boldsymbol{r})$, so that polarized excitation and detection can reveal polarized patterns of fluorescence, which then are used to reconstruct $\boldsymbol{n}(\boldsymbol{r})$ [2]. Label-free imaging of $\boldsymbol{n}(\boldsymbol{r})$ has also been realized by nonlinear optical microscopies based on multiphoton excitation, multi-harmonic generation, coherent anti-Stokes Raman scattering, and stimulated Raman scattering [3–5]. Despite their label-free character and other advantages in revealing micrometer-scale variations of $\boldsymbol{n}(\boldsymbol{r})$, these nonlinear optical imaging modalities exhibit limitations in resolution like that of conventional optical imaging. The grand challenge of optical studies of LCs is to optically probe $\boldsymbol{n}(\boldsymbol{r})$ with variation length scales considerably smaller than Abbe's diffraction limit [6], $\sim\lambda/2\mathrm{NA}$, with λ denoting wavelength of light and NA the numerical aperture of the objective. This corresponds to a resolution limit of 200–300 nm for visible light, which LC researchers could not overcome until now. We note that although the nonlinear nature of some of the previously utilized nonlinear imaging processes can slightly overcome the diffraction limit [3–5], these imaging techniques often rely on long-wavelength excitations, leaving the challenge of optical imaging of nanoscale director structures smaller than 200–300 nm not addressed. On the other hand, optical resolution up to 10s of nanometers has been achieved by the advent of super-resolution imaging techniques, including stimulated emission depletion (STED) microscopy [7,8], photoactivated light microscopy [9], and stochastic optical reconstruction microscopy [10,11], albeit with applications mainly in life science imaging and in material research where spatial patterns of position rather than orientation were probed.

In this Letter, we demonstrate super-resolution STED imaging of LC director structures by doping LCs with dye Nile Red, which has been identified as a dye suitable for both FCPM and STED [12–14]. In STED, fluorescence from excited fluorophores is reversibly switched off through depletion induced by stimulated emission [Fig. 1(a)]. When a donut-shaped STED beam is co-located with the excitation beam at the focus of the imaging system, fluorescence is depleted on the donut crust, resulting in a narrow super-resolution point spread function (PSF) [Fig. 1(c)]. In theory, the resolution scales with STED beam intensity I as $\lambda/(2\mathrm{NA}\sqrt{1+I/I_s})$ [15], where I_s is the saturation intensity. However, in practice, the resolution is often also limited by the dye photobleaching and sample photodamage. In this work, 5–15 mW of STED power was utilized, allowing us to overcome the diffraction limit in resolution while also mitigating the artifacts that could be caused

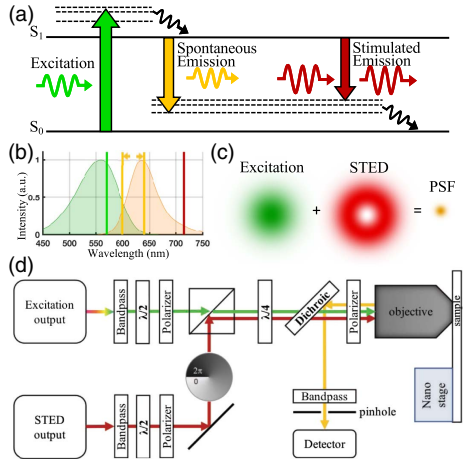

Fig. 1. Principles and implementation of STED polarizing microscopy (STED-PM). (a) Diagram illustrating the photophysical processes of fluorophores, including excitation, spontaneous emission, and stimulated emission. (b) Absorption and fluorescence spectra of Nile Red and the wavelengths and their ranges used in this work for excitation (570 nm), fluorescence detection (600–640 nm, as marked by orange arrows), and STED (715 nm). (c) Super-resolution PSF obtained by co-locating the donut-shaped STED beam and diffraction-limited excitation beam. (d) Simplified schematic of a STED polarizing microscope. A polarizer placed in an optical path right before the epi-detection objective enables polarized imaging and ensuing $\boldsymbol{n}(\boldsymbol{r})$ reconstruction based on polarization-dependent fluorescence textures. The laser pulse duration is ≈100 ps, and the repetition rate is 20 MHz.

by photobleaching and realignment of the director field due to the optical Frederiks transition [2–5]. Details of the STED imaging design are presented in Fig. 1, with the simplified schematic of a STED microscope [16] (modified to enable polarization sensitivity) shown in Fig. 1(d).

LC samples were prepared between two glass substrates, treated with 2 wt% aqueous solution of N,N-dimethyl-N-octadecyl-3-aminopropyltrimethoxysilyl chloride or polyimide (PI-2555, HD Microsystems) to set perpendicular (homeotropic) or tangential (planar) boundary conditions on the surfaces, respectively. The substrates were assembled into thin wedge cells with no spacers on one side (allowing for optical contact) and 2 μm spherical spacers on the other side. A short-pitch chiral nematic LC (LC without positional order) and a smectic A LC (LC with layered structure accompanying orientational order) 8CB (4-cyano-4′-octylbiphenyl, Frinton Laboratories, Inc., birefringence $\Delta n = 0.16$) were doped with 0.03 wt% of Nile Red and filled into the cells for imaging. The short-pitch chiral nematic LC was prepared by mixing 5 wt% of a chiral dopant $\alpha,\alpha,\alpha',\alpha'$-tetraaryl-1,3-dioxolane-4,5-dimethanol (TADDOL, Sigma-Aldrich) with a commercially available nematic mixture LC E7 (Slichem, China, $\Delta n = 0.23$), featuring a cholesteric pitch $p = 340$ nm measured by the cholesteric reflection spectra. To guide interpretation of the imaging results, numerical modeling of chiral nematic LC director structures based on minimization of bulk and surface elastic-free energy was performed. The minimization of Frank–Oseen free energy [1] supplemented by Rapini–Papoular anchoring potential [1,14] was performed for the experimental elastic constants of E7 ($K_{11} = 10.8$ pN, $K_{22} = 6.8$ pN, and $K_{33} = 17.5$ pN), the gap thickness of the LC cell of 50–200 nm, and the surface anchoring coefficient of 10^{-4} Jm^{-2}, with the numerical director relaxation approach described in detail elsewhere [17,18].

The FCPM image of the chiral nematic LC sample obtained with circularly polarized excitation and detection shows blurry cluster-like patterns on a dark background [Fig. 2(a)], while these clusters are clearly resolved as wiggly stripes of twist walls in the STED image with the same imaging polarization state and 5 mW STED power [Fig. 2(b)]. In both STED-PM and FCPM, the contrast in images arises from the sensitivity of both the dye's excitation and emission to the orientations of rod-like dye molecules that follow $\boldsymbol{n}(\boldsymbol{r})$ relative to the polarization state and propagation direction of STED-PM or FCPM light.

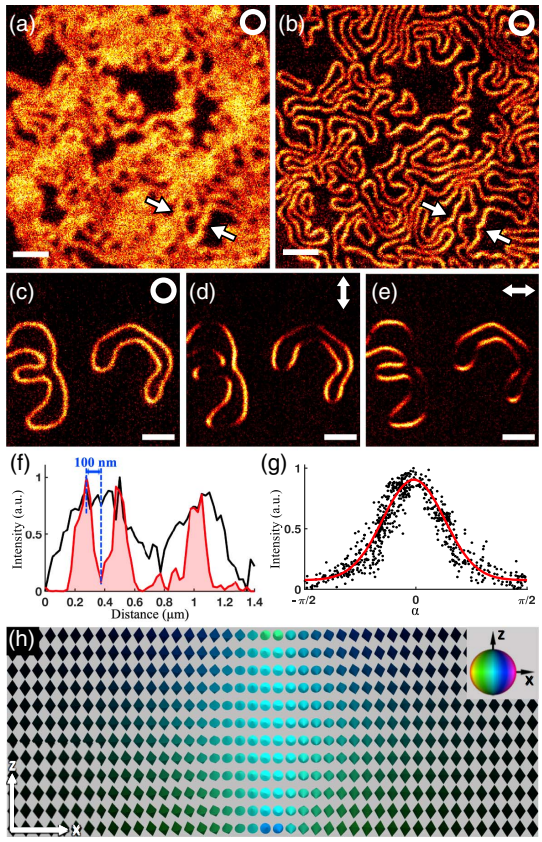

Fig. 2. Characterization of STED-PM and twist walls in chiral LCs. (a) Confocal and (b) STED images of Bloch walls in a chiral nematic LC probed with circularly polarized excitation/STED. The line intensity profile between the two arrows in (a) and (b) are shown in (f) in black and red, respectively, with the latter highlighted by filling the space below the curve for clarity. FWHMs of the peaks resolved by STED in (f) are 115 nm, 96 nm, and 131 nm (from left to right), while that in confocal imaging is 350 nm for the rightmost one. (c)–(e) STED images of the twist walls obtained with (c) circular and (d), (e) orthogonal linear polarizations reveal the dependence of polarized image intensity on α plotted in (g), and the red line is a guide to the eye. (h) Computer-simulated director structure in the vertical plane perpendicular to the wall visualized by double cones colored according to their orientations and the order-parameter sphere $\mathbb{S}^2/\mathbb{Z}_2$ with diametrically opposite points identified (shown in the upper-right inset). Polarizations are marked in the upper-right corners of (a)–(e). All scale bars are 1 μm. Here and elsewhere in the paper, the acquisition time was within 2–10 min.

STED-PM and FCPM fluorescence signals from the dye-doped LC with the director oriented out of the focal plane vary as $\propto \cos^4\theta$ (which is because the absorption and fluorescence both exhibit $\propto \cos^2\theta$ dependencies), where θ is the polar angle between the dye's molecular transition dipole and the focal plane. Therefore, both polarized luminescence images reveal that $\boldsymbol{n}(\boldsymbol{r})$ is in-plane in the central regions of the stripes and vertical in the LC background surrounding them, though STED-PM exhibits spatial resolution superior to that of FCPM. The normalized line profiles between the arrows in Figs. 2(a) and 2(b), obtained after subtracting the background, show substantial improvement in resolution, with the full width at half maximum (FWHM) of features reduced from 350 nm to 131 nm and features with a maximum and minimum separated by $\leq$100 nm distance resolved. This indicates imaging resolution better than 100 nm when accounting for the finite width of the actual fluorescent pattern due to the continuous rotation of the director within it. To compare the resolution between confocal and STED imaging of the LC director, we performed Fourier ring correlation analysis [19] on confocal images of the same field of view and obtained a resolution of (288 ± 3) nm. Therefore, at 5 mW STED power, an approximately threefold enhancement in STED over confocal imaging resolution is achieved. In dye-doped LCs, photobleaching is minimized, as the dye molecules can diffuse and replenish the imaged region [2]. Instead, the optical director realignment within LC structures under high-power illumination, known as optical Frederiks transition [2], sets the practical limit for laser power and STED resolution.

STED-PM images with collinearly polarized excitation, detection, and STED can resolve not only various angles of director tilt with respect to the sample's plane, but also reveal details of the azimuthal director orientation within these patterns. Linearly polarized STED-PM images in Figs. 2(d) and 2(e) reveal that the in-plane $\boldsymbol{n}(\boldsymbol{r})$ follows the direction of the stripes in their center. The image intensity versus the angle α between $\boldsymbol{n}(\boldsymbol{r})$ and linear STED-PM polarization is plotted in Fig. 2(g) by recording the intensity along the stripes in linear STED-PM images as a function of α. STED-PM intensity qualitatively shows a dependency somewhat stronger than $\propto \cos^4\alpha$, which would be expected for linear optical processes of absorption and luminescence for collinearly polarized excitation and detection. This strong angular sensitivity is likely enhanced by the polarization-dependent STED process and will require further studies. STED-PM images with different polarizations identify these stripes as Bloch walls, one type of the solitonic domain walls within which the director continuously rotates out of the plane of the sample [20]. Figure 2(h) shows the corresponding computer-simulated director structure of a LC Bloch wall where $\boldsymbol{n}(\boldsymbol{r})$ undergoes a smooth π twist across the wall to recover vertical orientation. In confined frustrated chiral LCs with perpendicular finite surface anchoring strength, such walls lower the free energy of the system as compared to the unwound background by enabling twist within them, consistent with our experiment and simulations.

Localized structures that appear as bright structureless spots are also observed in FCPM images of confined chiral nematic LC films [Fig. 3(a)]. In the corresponding STED image, these features are resolved as donut-like fluorescence patterns with a central dark region [Fig. 3(b)]. The peak-to-peak distance along a line passing through the center of the donut is 370 nm [Fig. 3(c)], making the detailed structure unresolved by FCPM with lateral resolution of ~300 nm. However, using the super-resolution STED-PM images shown in Figs. 3(d)–3(g), we can map out the in-plane orientation of $\boldsymbol{n}(\boldsymbol{r})$ and reconstruct it in Fig. 3(h). We visualize it by means of the preimages, spatial regions of $\boldsymbol{n}(\boldsymbol{r})$ orientations represented by the color in the order-parameter space in the insets of Figs. 3(j) and 3(k). The preimage pattern is consistent with that of a skyrmion, a two-dimensional topological soliton characterized by (in this case unity) skyrmion number, the topological charge that counts how many times $\boldsymbol{n}(\boldsymbol{r})$ wraps the order-parameter space [21,22]. The computer-simulated structure of a LC skyrmion is given in Figs. 3(j) and 3(k), showing the translational invariance in its field topology across the sample thickness. For a direct comparison, a computer simulated STED-PM image is shown in Fig. 3(i) (for resolution of 100 nm), closely matching its experimental counterpart.

LC structures studied in Figs. 2 and 3 are translationally invariant in nature, consistent with our modeling [Figs. 2(h) and 3(j), 3(k)]. However, in the case of much stronger surface anchoring or thicker cells, solitonic twist walls also can be

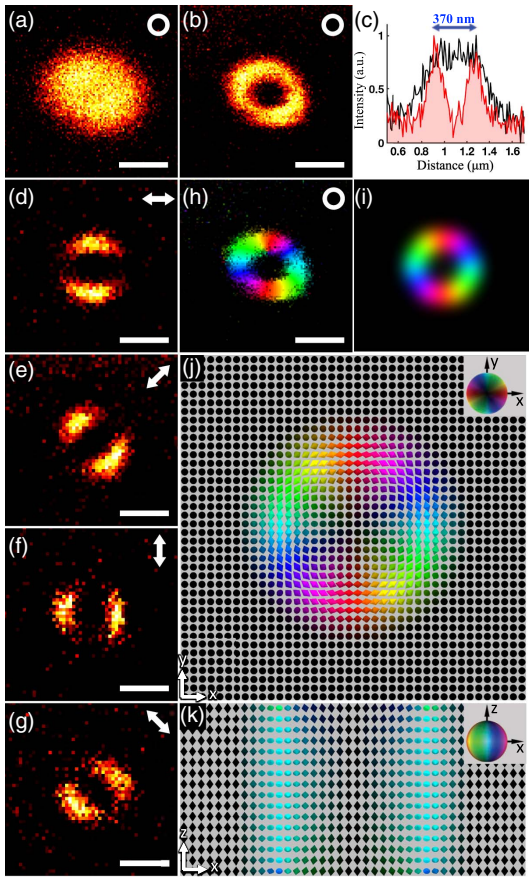

Fig. 3. Nanoscale LC skyrmions. (a) FCPM and (b) STED-PM images of a skyrmion. (c) Corresponding line profiles through the center of the skyrmion. (d)–(g) STED images taken with four different linear polarizations shown by double arrows. (h) Experimental reconstruction of director orientation within a skyrmion visualized by different colors [upper-right inset in (j)] and (i) its computer-simulated counterpart. (j), (k) Computer-simulated director field configuration of a skyrmion visualized by colored double cones in the (j) horizontal and (k) vertical planes. All scale bars are 300 nm.

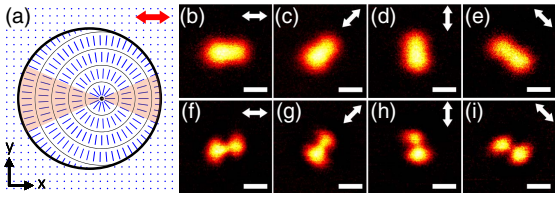

Fig. 4. STED-PM of defects in a smectic LC. (a) Schematic of the director structure of an FCD near the substrate with planar boundary conditions, where the blue rods and dots show the in-plane and vertical orientation of LC molecules, respectively. The thin black lines indicate the smectic layers, and thick black lines are the two singular lines along an ellipse and through its focus. The region colored red shows the expected fluorescence pattern for imaging with linear polarization marked in the upper-right corner. (b)–(i) Confocal [(b)–(e)] and STED-PM images [(f)–(i)] of an FCD for different linear polarizations. Scale bars are 300 nm.

accompanied by singular line defects near the substrates while forming one type of cholesteric fingers [22], while skyrmions can terminate on singular point defects near confining substrates to form the so-called "torons" [23]. The study of such three-dimensional structures with nanoscale super-resolution will require super-resolution PSF for not only the lateral directions, but also along the microscope's optical axis. This can be achieved using the so-called "z-donut" or "bottle" STED beams [8], but is beyond the scope of our present study.

The super-resolution STED-PM can be used to study other types of LCs, which we demonstrate by imaging focal conic domains (FCDs) in a smectic A LC. These defect structures in the layered organization of the smectic LC are common due to preserving layer equidistance within their volume and tend to form spontaneously in cells with hybrid (planar-homeotropic) boundary conditions [3]. The two-dimensional structure of an FCD near the substrate with planar surface boundary conditions is depicted in Fig. 4(a), where an elliptical singular line is formed on the surface of the substrate, and within which $\boldsymbol{n}(\boldsymbol{r})$ is radially outward from one of the foci with concentric smectic layers centered at the focus. Beyond the ellipse, $\boldsymbol{n}(\boldsymbol{r})$ is uniformly vertical. Analysis of the director structure indicates that the image focused near the planar substrate under linear polarization should be two circular sectors with their apices corresponding to one of the foci of the ellipse. Tiny FCDs were found in the thinner region of the wedge cell, and confocal images in Figs. 4(b)–4(e) show an elongated bright spot and the two circular sectors unresolved. In STED images with 10 mW of STED power in Figs. 4(f)–4(i), the two sectors are well resolved with an intensity dip in between, corresponding to the singular core at the focus of ellipse.

In conclusion, we have demonstrated STED super-resolution imaging of LC director fields in LCs. We have demonstrated that one-dimensional and two-dimensional topological solitons are ubiquitous when the cell thickness, cholesteric pitch, and anchoring extrapolation length (that quantifies competition between bulk and surface energy) are comparable and all in the range of ~100 nm. The achieved resolution of orientational STED microscopy is three times better than that of confocal imaging, revealing LC structures previously unresolved by existing diffraction-limited microscopies. The resolution can potentially be further improved by optimizing selection of dyes or increasing STED power while enhancing the stability of LC structures, for example, by polymer stabilization. Super-resolution imaging capability of the LC director may provide means of probing rich structures and polymesomorphism of LCs at length scales smaller than the optical diffraction limit, including LC blue phases and twist-bend nematic phase. Incorporating the super-resolution capability in the axial dimension will be an important next step towards full 3D super-resolution imaging of director fields. Beyond LCs, our nanoscale orientation-sensitive imaging approach can be extended to polymers, active matter systems, colloids, membranes, and various other soft matter and biological systems with orientational ordering [1]. Similar to FCPM [2] and nonlinear optical microscopies [3–5], in addition to photobleaching and laser-induced realignment, STED-PM studies require special precautions to avoid artifacts associated with changes in polarization of imaging light in thick LC samples, absorption-mediated temperature change, defocusing, scattering of light caused by director fluctuations, inhomogeneities in spatial distribution of dye molecules, etc.

Funding. National Science Foundation (NSF) (DMR-1810513, support of research); National Institutes of Health (NIH) (S10 RR023381, support of facilities).

Acknowledgment. We acknowledge assistance and discussions with T. Lee, S. Meyer, P. Ackerman, T.-W. Hsu, and D. Stich.

REFERENCES

1. P. M. Chaikin and T. C. Lubensky, *Principles of Condensed Matter Physics* (Cambridge University, 2000).
2. I. I. Smalyukh, S. V. Shiyanovskii, and O. D. Lavrentovich, Chem. Phys. Lett. **336**, 88 (2001).
3. T. Lee, R. P. Trivedi, and I. I. Smalyukh, Opt. Lett. **35**, 3447 (2010).
4. A. V. Kachynski, A. N. Kuzmin, P. N. Prasad, and I. I. Smalyukh, Appl. Phys. Lett. **91**, 151905 (2007).
5. T. Lee, H. Mundoor, D. G. Gann, T. J. Callahan, and I. I. Smalyukh, Opt. Express **21**, 12129 (2013).
6. E. Abbe, Arch. für mikroskopische Anat. **9**, 413 (1873).
7. S. W. Hell and J. Wichmann, Opt. Lett. **19**, 780 (1994).
8. T. A. Klar, S. Jakobs, M. Dyba, A. Egner, and S. W. Hell, Proc. Natl. Acad. Sci. USA **97**, 8206 (2000).
9. E. Betzig, G. H. Patterson, R. Sougrat, O. W. Lindwasser, S. Olenych, J. S. Bonifacino, M. W. Davidson, J. Lippincott-Schwartz, and H. F. Hess, Science **313**, 1642 (2006).
10. M. J. Rust, M. Bates, and X. Zhuang, Nat. Methods **3**, 793 (2006).
11. S. T. Hess, T. P. K. Girirajan, and M. D. Mason, Biophys. J. **91**, 4258 (2006).
12. G. Moneron and S. W. Hell, Opt. Express **17**, 14567 (2009).
13. M. Vitek and I. Muševič, Opt. Express **23**, 16921 (2015).
14. I. I. Smalyukh, Mol. Cryst. Liq. Cryst. **477**, 23 (2007).
15. V. Westphal and S. W. Hell, Phys. Rev. Lett. **94**, 143903 (2005).
16. S. A. Meyer, B. N. Ozbay, M. Potcoava, E. Salcedo, D. Restrepo, and E. A. Gibson, J. Biomed. Opt. **21**, 066017 (2016).
17. P. J. Ackerman and I. I. Smalyukh, Phys. Rev. X **7**, 011006 (2017).
18. M. Ravnik and S. Žumer, Liq. Cryst. **36**, 1201 (2009).
19. G. Tortarolo, M. Castello, A. Diaspro, S. Koho, and G. Vicidomini, Optica **5**, 32 (2018).
20. M. Kleman, *Points, Lines and Walls: In Liquid Crystals, Magnetic Systems and Various Ordered Media* (Wiley, 1983).
21. N. Nagaosa and Y. Tokura, Nat. Nanotechnol. **8**, 899 (2013).
22. P. J. Ackerman, R. P. Trivedi, B. Senyuk, J. van de Lagemaat, and I. I. Smalyukh, Phys. Rev. E **90**, 012505 (2014).
23. I. I. Smalyukh, Y. Lansac, N. A. Clark, and R. P. Trivedi, Nat. Mater. **9**, 139 (2010).